

## Experimental study on temperature evolution of pseudoelasticity TiNi alloys during shock-induced phase transformation

L. SHEN<sup>1)</sup>, Y. LIU<sup>1,2)</sup>, J. SHAN<sup>2)</sup>

<sup>1)</sup>*Department of Engineering Mechanics  
School of Civil Engineering  
Henan Polytechnic University  
Jiaozuo, Henan 454000, China*

<sup>2)</sup>*CAS Key Laboratory of Mechanical Behavior  
and Design of Materials  
Department of Modern Mechanics  
University of Science and Technology of China  
Hefei, Anhui 230027, China  
e-mail: liuyongg@hpu.edu.cn*

THE TEMPERATURE EVOLUTION AND THE MECHANICAL CHARACTERISTICS of pseudoelasticity TiNi alloys have been studied experimentally at different strain rates. During SHPB testing, the temperature changes were in situ measured by an infrared system recording infrared radiation emitted from the surface of the specimen. It was found that the temperature evolution and the mechanical behavior has a remarkable strain rate effect. With the strain rate increasing, both phase transition subsequent stress and modulus of loading the phase transition stage were higher, exhibiting significant strain and the strain rate hardening characteristic. They were accompanied by the temperature increasing, which suggest that the stress increments result from the temperature change, independently of the strain rate. Calculation analysis results show that latent heat and the dissipated energy in the form of the hysteresis loops, are mainly the sources of the temperature change.

**Key words:** temperature evolution, phase transformation, infrared radiation, strain rate, in situ.

Copyright © 2018 by IPPT PAN

### 1. Introduction

SHAPE MEMORY ALLOYS (SMAS), such as TiNi, are functional materials and have been widely used in a variety of engineering applications due to their unique shape memory effects (SME) and pseudoelasticity (PE), which originate from a thermoelastic martensitic phase transition between two crystalline phases, called austenite (A, high temperature stable phase) and martensite (M, low

temperature stable phase) [1–3]. The formation of martensite can be induced either by temperature (i.e., cooling below the martensite start temperature) or by stress (i.e., by loading above a critical stress level). The PE response, in particular, refers to the fact that rather large strains (up to 8%) can be imposed by mechanical loading and then recovered upon unloading, albeit via a stress hysteresis loop.

The previous research on the mechanical behavior of pseudoelasticity TiNi alloys has mainly concentrated on quasi-static loading conditions. It was observed in many experiments [4–8] that the stress hysteresis strongly depended on the strain rate. A few researchers reported that the changes in mechanical properties are due to the temperature change by latent heat of martensitic transformation [9–14]. Physically, under a given strain rate, the localized release/absorption of the latent heat during the forward/reverse phase transition process gives rise to the swift temperature variation and heat transfer in a material. In turn, the temperature variations will have an influence on the phase transformation process since the transformation stress is depended on the temperature [6, 9, 14, 15]. Therefore, thermo-mechanical coupling is inherent in the phase transition and will significantly influence the behavior of the material. In principle, the higher the strain rate, the less time to transfer the latent heat and therefore, the stronger the thermo-mechanical coupling effect. For better understanding the relation between the strain rate and thermo-mechanical coupling, the temperature evolution in the process of phase transformation is a key issue, which can be calculated by mathematical skills involving complicated transient heat transfer and multiple moving heating sources [6]. The other way is to directly measure the change of temperature during the phase transition.

From experimental point of view, infrared radiation thermography (IRT) have been widely used in the fields of static and dynamic mechanics [16–20], because of reasonable accuracy, non-contact technique, low-cost developments, no or less damage on testing objects. For the phase transformation process, SHAW and KYRIAKIDES [9] performed experiments of SMAs in air and in water. Their results show a stronger dependence of the mechanical behavior on loading rates in the air than in water suggesting that this dependence is due to the thermo-mechanical coupling effect. SUN *et al.* [15] showed experimentally that the number of nucleation and propagation speed of the new phase band is depended on temperature and the temperature evolves non-monotonically with the loading rate. In the work of GRABE and BRUHNS [23], this dependence disappears completely when the temperature of the test sample is kept constant revealing the fact that this dependence lies in the temperature effect rather than a strain rate effect. A similar conclusion can be also seen in GADAJ *et al.* [21, 22]. The above studies are all mainly focused on quasi-static conditions (low strain rate). In fact, IRT is only applicable to the low strain rate condition because of

its low time response, however, apart from CHEN and SONG [24], who measured the temperature change in NiTi alloy by a thermocouple, there are no experimental studies on the temperature evolution of PE NiTi under shock loading at relatively high strain rates (of the order  $10^2 \sim 10^3 \text{s}^{-1}$ ).

The present paper is to carry out the shock compression characterization of PE TiNi alloy, by a conventional Split Hopkinson Pressure Bar (SHPB) apparatus with an infrared temperature measurement system (ITMS) to obtain the nature and properties of the temperature evolution in the process of phase transformation. This work is intended as a step towards understanding the influence of thermo-mechanical coupling on the behavior of PE SMAs by analyzing the temperature change effect on the mechanical response characteristics.

## 2. Experimental procedure

### 2.1. Materials and specimens

The material considered in this study is a commercial polycrystalline TiNi alloy with a nominal composition of 50.9 at % Ni balanced with Ti (Nitinol Devices & Components, USA), exhibiting PE behavior at room temperature ( $24.4^\circ\text{C}$ ). Characteristic temperature parameters measured by the DSC test and other thermo-mechanical properties are listed in Table 1. The specimen geometry is in the form of cylinder with the length 6 mm and 8 mm in the diameter. An optical micrograph of a PE TiNi indentation sample depicting its microstructure is shown in Fig. 1. The figure reveals an un-uniform equiaxed grain structure, with an average grain size of  $15\sim 20 \mu\text{m}$ .

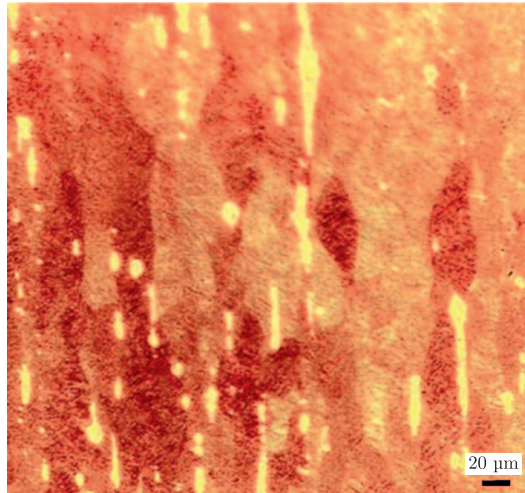


FIG. 1. Microstructures of the specimen.

**Table 1. Thermodynamic parameters of TiNi alloy specimens<sup>\*)</sup>.**

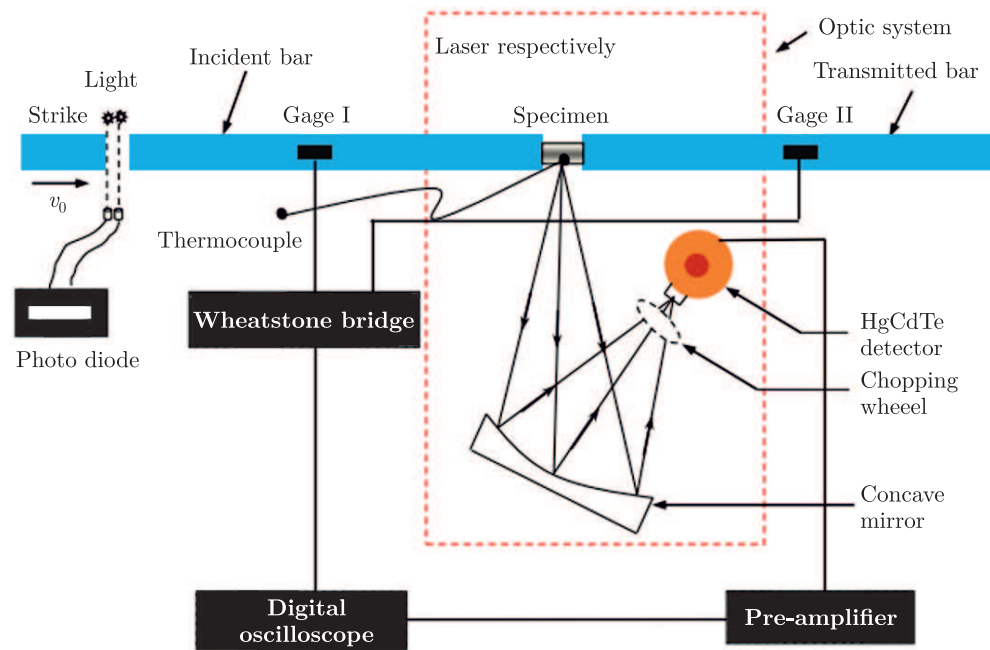
Parameters	Value
$\rho$ (kg/m <sup>3</sup> )	6450
L (J/g)	8.77
$C_P$ (J/g/°C)	0.45
$M_s$ (°C)	-27.4
$M_f$ (°C)	-48.5
$A_s$ (°C)	-26.6
$A_f$ (°C)	-9.2
$\epsilon_{tr}$	48%

<sup>\*)</sup>  $\rho$  – density, L – latent heat,  $C_P$  – specific heat,  $M_S/M_f$  and  $A_S/A_f$  – start/finish temperatures for martensitic and austenite transitions, respectively,  $\epsilon_{tr}$  – phase transformation completion strain.

## 2.2. Experiment setup

A schematic illustration of the experimental setup is shown in Fig. 2. The experimental setup consists of two parts: one is SHPB, which has been widely used to characterize the dynamic properties of materials under the high strain rate loading, and the other is ITMS. In the SHPB system, the striker, the incident bar and the transmission bar were steel with the diameter 14.5 mm and length 20 mm, 2000 mm and 2000 mm, respectively. During a test, the specimen is sandwiched between the incident and transmission bars. Both ends of the specimen are greased to reduce the end-friction effect on the specimen deformation during the dynamic test. The striker bar impacts the incident bar and generates in it an elastic stress pulse whose width is twice the length of the striker bar. The incident pulse on reaching the sample is partly reflected back in the incident bar as tension and is partly transmitted through the sample into the transmission bar, which is measured by the strain gauges on the incident and transmission bars. These signals were recorded by a high-speed digital oscilloscope, i.e. Tektronix TDS3084 with the acquisition frequency 10.0 MS/s. According to the one dimensional theory of elastic wave propagation [25], the stress-strain curves of the material are calculated based on the three-wave method.

The red dotted lines in Fig. 2 represented the ITMS, the most important of which is a 1 mm×1 mm HgCdTe detector element (Mercury Cadmium Telluride) photovoltaic photon detector (J15D12-M204-S01M-60, Judson Co., USA). For the HgCdTe element used, the maximum responsivity covers wave-lengths of 8–12  $\mu\text{m}$ , which correspond to a black body temperature between 300 and 400 K, i.e. the range expected in our experiments. The temperature resolution of the array (as will be seen subsequently) is of the order of 0.1 K. To obtain such a resolution, the signal to noise ratio for the HgCdTe elements must be maximized,



a) Schematic illustration of the experimental setup

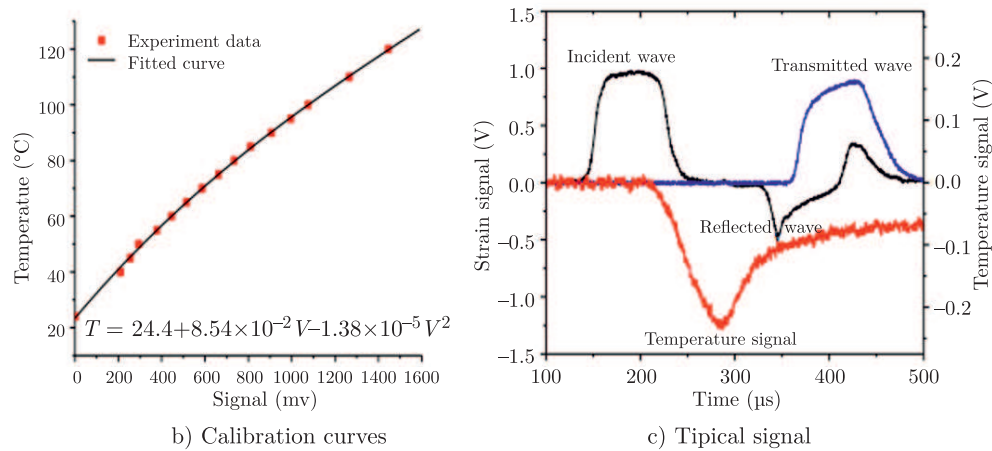


FIG. 2. Experimental setup for the thermo-mechanical characterization at impact.

which is done by placing the detectors in the 77 K liquid nitrogen bath. Radiation emitted from the surface of a specimen as it deforms and heats up is forced onto the detector element by a gold coated concave mirror with the focal length 200 mm and the effective diameter 50mm. The ray diagram for the focusing optics is shown in Fig. 2. The detector's response is connected to the oscilloscope

via its amplifier (PA-101, Judson Co.) with bandwidth 10 Hz–1 MHz, the output of which are fed into a bank of eight multiplexers. The multiplexed signals are then digitized using four 2-channel, Gage 1012A/D boards, running at speeds up to 10MHz. The system rise time is approximately 0.5  $\mu$ s. The more details of each of the components of the system and the results of some preliminary applications of the system are given in ZEHNDER *et al.* [18].

### 2.3. Calibration

Because the output of the infrared detectors is always in the form of voltage, a calibration between output voltage and temperature has to be established. In theory, the relation between the detector voltage measurement and the actual temperature can be found, if the emissivity of the surface is known [26]. Unfortunately, such a relation is not easy to establish because the specimen's emissivity and the detector's spectral responsivity are very difficult to measure. Therefore, an experimental calibration was carried out instead. Calibration of the system is performed in a direct manner. Since the ITMS system is only sensitive to AC signals, a chopping wheel is placed between the specimen and the detector to transfer a quasi-static signal into an A.C. signal. Before calibration, a K-type thermocouple was inserted into a small hole drilled on the lateral surface of the specimen as close as possible to the opposite lateral surface. A specimen when tested, is heated to a temperature above the expected maximum temperature of the actual tests by an alcohol lamp. A laser beam is used to position the calibration specimen which can keep the same position for impact tests. After that the alcohol lamp is removed, as the sample cools, the voltage output from the infrared detectors element is recorded by the data acquisition system along with the sample temperature. This procedure provides a voltage vs. temperature curve. A typical calibration curve for a TiNi alloy specimen is shown in Fig. 2b. Curve fitting shows that the relation between the temperature and the voltage is usually a second order polynomial. Since the surface texture of the specimen affects emissivity, it is important to maintain the same specimen preparation technique throughout all experimentation.

Great care should be taken into account during the calibration procedure since any errors made at this stage are directly reflected in the final measurements. According to KAPOOR and NEMAT-NASSER [27], infrared calibrations made in this way may lead to measurements underestimating the conversion ratio. One possible reason for the underestimation, they suggested, is that during the slow calibration procedure the atmosphere around the specimen is also heated, which itself adds to the IR radiation measured by the detectors. In contrast, during the actual test where the whole event lasts less than 200  $\mu$ s, the surrounding atmosphere does not contribute any IR radiation. Their assertion is,

in effect, that the emissivity of air is non-negligible. To investigate this assertion for our infrared HgCdTe detectors a furnace was heated up to 200°C and the identical setup used above was focused in the interior of the (empty) furnace. Virtually no signal was recorded on the detectors (compared to actual temperatures recorded in the experimentation). Hence, the contribution from air infrared radiation emission during calibration is negligible, at least for the detectors and electronics used in the present study. The effect of oxidation of the specimen on its emissivity when heated was also discussed by GUDURU *et al.* [19], it was concluded that there was no oxidation up to 250°C.

During the experiment, the strain gauge on the incident bar, which upon impact triggers the laser pulses, also triggers the data acquisition system for the IR system. Figure 2c shows a typical signal of the original strain wave and infrared detector. The temperature response can be obtained by converting infrared detector signals in the form of voltage using the fitted formula, while the stress-strain curves are obtained from the strain wave records based on one dimensional stress wave theory [29].

### 3. Experimental results and analysis

Three tests were performed, and three different striker velocities, 10.2 m/s, 14.5 m/s and 17.8 m/s are considered corresponding to strain rates of 550, 890 and 1450/s, respectively. The concrete experimental conditions and main results are listed in Table 2. It is clearly shown that when the force was removed, most of the strain was recovered but small residual deformation remained. This may be due to a small increase of dislocation density and the stabilization of amounts of residual martensite. In fact, when the recuperated samples were placed in hot water (80~100°C) for about 30 minutes, most of these residual could be recovered, implying that the majority residual strain is the elastic deformation of martensitic grains, which could be converted into the austensite phase when heated.

**Table 2. Experimental conditions and main results**

Test	Impact velocity (m/s)	Strain rate (s <sup>-1</sup> )	Phase transition threshold stress(Mpa)	Maximum temperature (°C)	Residual strain
#1	10.2	550	570	33.1	0.6%
#2	14.5	890	585	43.3	1.0%
#3	17.8	1450	612	51.1	1.2%

Figure 3 presents the variation of the stress as a function of the strain for different strain rates and the corresponding temperature change versus time.

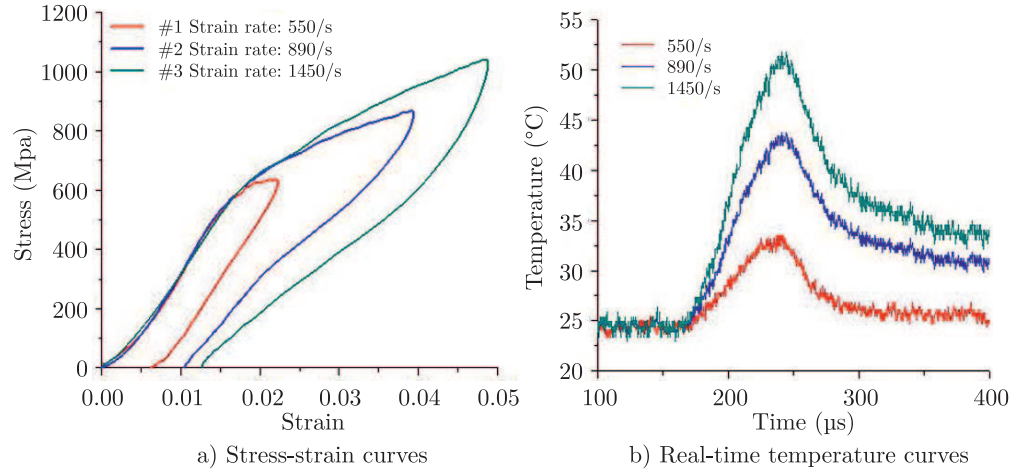


FIG. 3. Stress-strain curves and temperature history.

Comparing Fig. 3(a) with (b), two important observations are made: during forward/reverse phase transformation, temperature increases/decreases, and the temperature change has a remarkable strain rate effect. During unloading, the temperature decreases, and reaches a value higher than the initial temperature after unloading. Physically, this can be explained by the predominance of latent heat with respect to other heat sources during phase transformation. More precisely, as shown in Fig. 4, there are obviously three stages in the process of temperature with the strain increasing:

- 1 stage (O-A in stress-strain curve, O-D in temperature). This stage is conventionally attributed to the elastic distortion of the austenite lattice. A slight temperature increase is observed, ranging from  $1.5^{\circ}\text{C}$ ,  $2.7^{\circ}\text{C}$  to  $5.4^{\circ}\text{C}$  corresponding to the strain rate 550/s, 890/s and 1450/s. In principle, for the specimen, as an elastic shock wave passes through, the material is homogeneously compressed in the shocked direction. However, due to a geometric discontinuity or a crystal particle, stress concentrations arise and local phase transition deformation occurs when a certain threshold stress is reached. Thus, a local temperature increase comes into being at those locations of in-homogeneities. This increase in temperature, in turn, has a stabilizing effect against further transformation, so critical stress of the transformation phase was improved by 570 Mpa, 585 Mpa and 612 Mpa with the strain rate increasing from 550/s, 890/s to 1450/s. Moreover, during this stage deformation, small defects may arise even at the elastic range due to the high stresses developed at impact. This may explain the small plastic strain after the test.

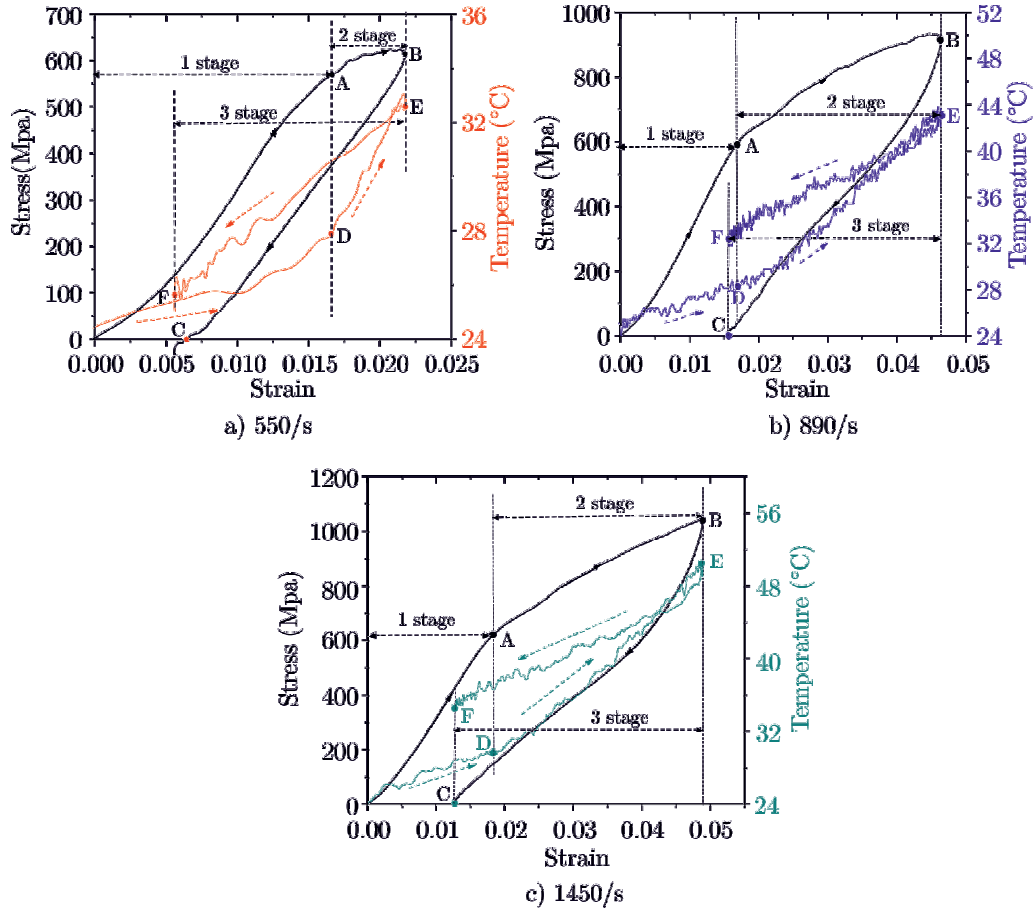


FIG. 4. Typical stress and temperature vs. strain for different strain rate.

- 2 stage (A-B in stress-strain curve, D-E in temperature). From the engineering stress and strain curves, it is shown that this stage is associated with the martensite phase transformation deformation over a positive slope of the stress-strain curve. Slopes of 5.5 Mpa, 9.7 Mpa and 12.2 Mpa correspond to the strain rate of 550/s, 890/s and 1450/s respectively, exhibiting remarkably the strain hardening effect, which may be explained by the evolution of the temperature measurements in this stage. The temperature increases non-linearly with the increasing phase transition strain, and up to its maximum value, 33.1°C, 43.3°C and 51.1°C at strain rates of 550/s, 890/s and 1450/s, respectively.
- 3 stage (B-C in stress-strain curve, E-F in temperature). This stage is conventionally seen as the elastic unloading and reverse phase transition

unloading deformation. The temperature decreases continuously in this stage. In fact, once unloading, the martensite phase is unstable and is converted into an austenite phase by absorbing heat, thus leading to a decrease of the specimen temperature. That is to say, there is an inverse phase transition in the process of elastic unloading, which is similar to elastic loading. So, no clear distinction point in the stress-strain curve between elastic unloading and the reverse transition stress is observed. After a cycle of loading/unloading, the temperature is higher than the initial value (24.4°C) depending on the strain rate, 26.0°C, 32.4°C and 34.7°C at the strain rate of 550/s, 890/s and 1450/s, respectively.

#### 4. Discussion

As discussed in Section 3, there exists temperature variation during the shock induced phase transformation. Neglecting any heat source of external origin, heat transfers are governed by the following local heat conduction equation:

$$(4.1) \quad \rho C_p \dot{T} - k \text{lap} T = \dot{Q}$$

where  $T$  and  $\dot{T}$  is the specimen temperature and its rate at any point of the body, respectively. The terms of ‘lap  $T$ ’ stands for the laplacian operator applied to the temperature field. It is assumed that the heat conduction is governed by the standard Fourier’s law with an isotropic, uniform and constant thermal conductivity  $k$ . The terms  $\rho$  and  $C_p$ , denote the mass density, specific heat, respectively, which are both assumed to be uniform and constant.  $\dot{Q}$  is the specific heat source rate.

For the shock loading, the thermal conductivity effect and the heat convection with external environment can be neglected, so Eq. (4.1) is simplified to

$$(4.2) \quad \rho C_p \dot{T} = \dot{Q}.$$

It is well known that deformation mechanisms for NiTi SMAs include elastic distortion of the atomic lattice and additional mechanisms associated with martensitic transformation [9]. The heat source rate  $\dot{Q}$  involved in Eq. (4.2) is thus divided into three parts: the first rate  $\dot{Q}_{\text{tr}}$  due to latent heat, the second one  $\dot{Q}_{\text{diss}}$  due to the intrinsic dissipations induced by irreversible phenomena, such as plasticity and frictional barriers, opposing interfacial motions and the third one  $\dot{Q}_{\text{thel}}$  due to the usual thermoelastic coupling

$$(4.3) \quad \dot{Q} = \dot{Q}_{\text{tr}} + \dot{Q}_{\text{diss}} + \dot{Q}_{\text{thel}} \quad \text{with } \dot{Q}_{\text{thel}} = -\alpha T \dot{\sigma}, \quad \dot{Q}_{\text{diss}} = \sigma \dot{\epsilon}_{\text{ph}}$$

where  $\alpha$  is the thermal expansion coefficient.

According to the classical additive decomposition of the strain, the strain rate is written as following:

$$(4.4) \quad \dot{\epsilon} = \dot{\epsilon}_{el} + \dot{\epsilon}_{in}$$

where  $\dot{\epsilon}_{el}$  and  $\dot{\epsilon}_{in}$  are the elastic and inelastic strain rates, respectively. The inelastic strain rate includes the phase transformation deformation  $\dot{\epsilon}_{tr}$  and the rate due to plastic deformation. In the present work, the last is neglected.

In the work of LEXCELLENT and VACHER [28], both strain rate  $\dot{\epsilon}_{tr}$  and heat source rate  $\dot{Q}_{tr}$  could be assumed proportional to the transformation fraction rate  $\dot{f}$

$$(4.5) \quad \dot{\epsilon}_{tr} = \dot{f}\epsilon_{tr} \quad \text{and} \quad \dot{Q}_{tr} = \dot{f}L$$

where  $\epsilon_{tr}$  and  $L$  stand for the transformation strain and latent heat for a complete transformation ( $f = 1$ ), about 4.8% and 8.77 J/g, respectively, as shown in Table 1.

Combining Eqs. (4.2)–(4.5) results in

$$(4.6) \quad \rho C_p \dot{T} = -\alpha T \dot{\sigma} + L \dot{f} + f \dot{\epsilon}_{tr}.$$

The observed temperature increase starting for very low stress during the 1 stage suggests an additional deformation mechanism involving an exothermic phase transformation. A pure elastic deformation would lead to a homogeneous temperature decrease associated with the well-known thermo-elastic coupling, as revealed by Eq. (4.3), which leads to  $\dot{Q}_{thel} < 0$  when  $\dot{\sigma} > 0$ .

The temperature changes calculated by formula (4.3) are presented in Fig. 5 as functions of a strain rate. Figure 5 shows that the increase in temperature

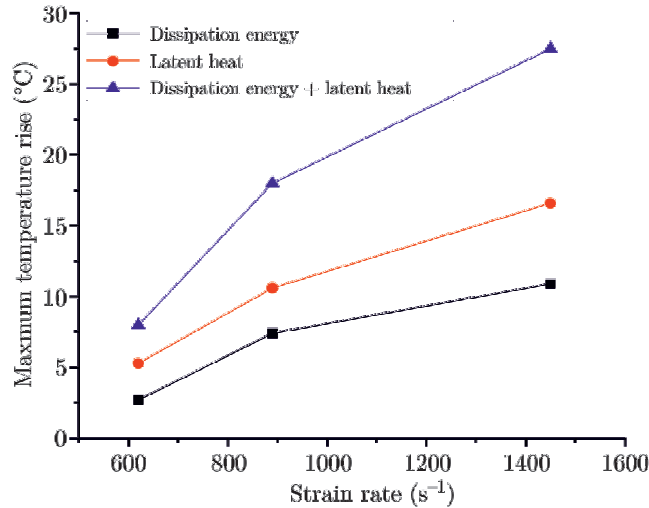


FIG. 5. Latent heat and dissipated energy effect on the temperature change.

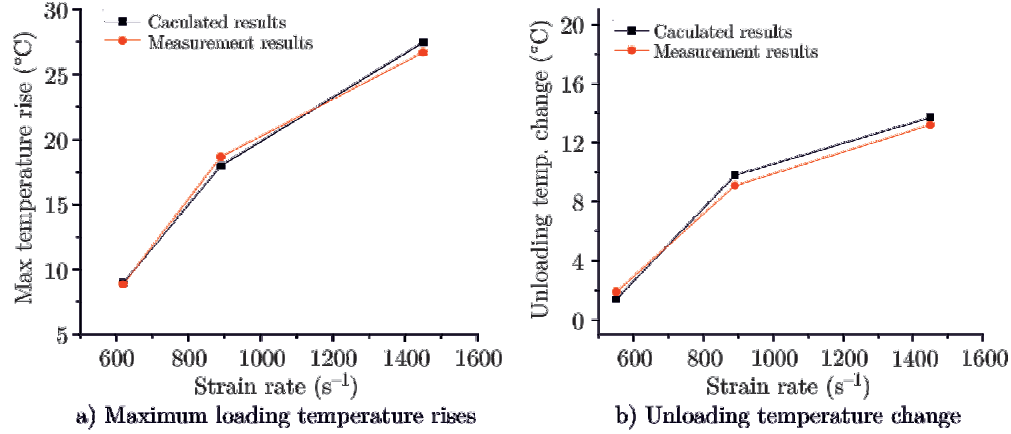


FIG. 6. Temperature change calculated.

induced by dissipation energy is more than one third of the total temperature rise, suggesting that the effect of dissipation work on the temperature change cannot be ignored. Not only that, this dissipation energy can be lived, which will influence the specimen temperature after a cycle of loading /unloading. Moreover, the ultimate temperature is not only dependent on the dissipation work, but also is controlled by the residual phase transition strain. The maximum temperature rise and the ultimate temperature calculated by formula (4.3) are in good agreement with the experimental measurement results, as shown in Fig. 6. The slight difference between the two results may lie in two reasons, one is that the conversion factor  $\alpha$  is difficult to determine, often an empirical value, the other may be related to the phase transformation strain, especially for the residual phase change strain.

## 5. Conclusions

In this paper, infrared radiation technology has been applied to detect in situ temperature evolution in the process of shock loading induced phase transformation of PE TiNi alloy specimens. Several conclusions are as follows:

1. Elastic and phase transformation deformation during shock loading and unloading are often accompanied by the significant temperature changes. And these temperature changes have the remarkable strain rate effect, which is mainly shown in the maximum temperature and the temperature after unloading increasing with the increase in the strain rate.

2. The temperature evolution could be generally divided into three stages. Initially, the temperature increased slightly due to a local stress concentration. Secondly, the temperature rapid rise resulted from the release of latent heat

and the hysteresis dissipation energy associated with the stabilized state of the stress-strain response. Finally, the temperature dropped during the cycle of loading/unloading owing to the fact that reverse phase transition endothermic, and residual phase transformation deformation.

3. The change in temperature in turn affects the properties of the material. The temperature effect is mainly reflected in two aspects. One is the hardening effect, manifested in the slope of a mixed phase in the stress-strain relation increases with the strain rate, in essence, which lies in the phase transition stress relevance to the temperature. The other is that the dissipation energy in the form of the hysteresis loop area of stress-strain curves increases with the strain rate, which is related to the loop and the strain increasing. In truth, the strain rate effect and the temperature effect are coupled with each other.

The main lack of these experimental results and analysis is the assumption of homogeneous deformation, which becomes increasingly important for the temperature measurement of a small area in the specimen surface. Stress uniformity for SHPB technology does not mean the deformation uniform, especially in the crystal scale. In fact, in this paper, the phenomenon of the slight temperature change during elastic deformation of an austenite phase fully reflects that there exists the local phase transition deformation. Therefore, further research should be directed to take the phase transition wave propagating in the specimen and linear array or area zones of the temperature measuring system into account.

### Acknowledgements

This study was supported financially by the National Natural Science Foundation of China (11072240,11702086) and the Ph.D. Funding Support Program of the Henan Polytechnic University.

### References

1. R. ABEYARATNE, J.K. KNOWLES, *A continuum model of a thermoelastic solid capable of undergoing phase transitions*, Journal of the Mechanics and Physics of Solids, **41**, 541–571, 1993.
2. L. DELAEY, R.V. KRISHNAN, H. TAS, H. WARLIMONT, *Review thermoelasticity, pseudoelasticity and the memory effects associated with martensitic transformations, Part 1. Structural and microstructural changes associated with transformations*, Journal of Materials Science, **9**, 1521–1535, 1974.
3. J.A. SHAW, *Simulations of localized thermo-mechanical behavior in a NiTi shape memory alloy*, International Journal of Plasticity, **16**, 541–562. 2000.
4. M.A. IADICOLA, J.A. SHAW, *Rate and thermal sensitivities of unstable transformation behavior in a shape memory alloy*, International Journal of Plasticity, **20**, 577–605, 2004.

5. G.N. DAYANANDA, M. SUBBA RAO, *Effect of strain rate on properties of superelastic NiTi thin wires*, Materials Science and Engineering A, **486**, 96–103, 2008.
6. P.H. LEO, T.W. SHIELD, O.P. BRUNO, *Transient heat transfer effects on the pseudoelastic behavior of shape-memory wires*, Acta Metallurgica et Materialia, **41**, 8, 2477–2485, 1993.
7. C. ELIBOL, X. WAGNER, *Strain rate effects on the localization of the stress-induced martensitic transformation in pseudoelastic NiTi under uniaxial tension, compression and compression–shear*, Materials Science and Engineering A, **643**, 194–202, 2015.
8. X.H. ZHANG, P. FENG, Y.J. HE, T.X. YU, Q.P. SUN, *Rate dependence of macroscopic domain patterns in stretched NiTi strips*, International Journal of Mechanical Sciences, **52**, 1660–1670, 2010.
9. J.A. SHAW, S. KYRIAKIDES, *Thermo-mechanical aspects of NiTi*, Journal of the Mechanics and Physics of Solids, **43**, 8, 1243–1281, 1995.
10. P.G. McCORMICK, Y. LIU, S. MIYAZAKI, *Intrinsic thermal-mechanical behavior associated with the stress-induced martensite transformation in TiNi*, Materials Science and Engineering A, **167**, 51–56, 1993.
11. F. AURICCHIO, E. SACCO, *Thermo-mechanical modeling of superelastic shape memory wire under cyclic stretching-bending loadings*, International Journal of Solids and Structures, **38**, 6123–6145, 2001.
12. L. ANAND, M.E. GURTIN, *Thermal effects in the superelasticity of crystalline shape memory materials*, Journal of the Mechanics and Physics of Solids, **51**, 1015–1058, 2003.
13. C. MORIN, Z. MOUMNI, W. ZAKI, *Thermomechanical coupling in shape memory alloys under cyclic loadings: Experimental analysis and constitutive modeling*, International Journal of Plasticity, **27**, 1959–1980, 2011.
14. O.P. BRUNO, P.H. LEO, F. REITICH, *Free boundary conditions at austenite-martensite interfaces*, Physical Review Letters, **74**, 746–749, 1995.
15. Q.P. SUN, Z.Q. LI, *Phase transformation in superelastic NiTi polycrystalline micro-tubes under tension and torsion—from localization to homogeneous deformation*, International Journal of Solids and Structures, **39**, 3797–3809, 2002.
16. J.J. MASON, A.J. ROSAKIS, G. RAVICHANDRAN, *On the strain and strain rate dependence of the fraction of plastic work converted into heat: an experimental study using high-speed infrared detectors and the Kolsky bar*, Mechanics of Materials, **17**, 135–145, 1994.
17. P.R. GUDURU, A.J. ROSAKIS, G. RAVICHANDRAN, *Dynamic shear bands: an investigation using high speed optical and infrared diagnostics*, Mechanics of Materials, **33**, 371–402, 2001.
18. A.T. ZEHNDER, A.J. ROSAKIS, *On the temperature distribution at the vicinity of dynamically propagating cracks in 4340 steel*, Journal of the Mechanics and Physics of Solids, **39**, 385–415, 1991.
19. P.R. GUDURU, A.T. ZEHNDER, A.J. ROSAKIS, ET AL., *Dynamic full field measurements of crack tip temperatures*, Engineering Fracture Mechanics, **68**, 14, 1535–1556, 2001.
20. R. KOMANDURI, Z.B. HOU, *Thermal modeling of the metal cutting process-Part III: temperature rise distribution due to the combined effects of shear plane heat source and the tool–chip interface frictional heat source*, International Journal of Mechanical Sciences, **43**, 1, 89–107, 2001.

21. S.P. GADAJ, W.K. NOWACKI, H. TOBUSHI, *Temperature evolution during tensile test of TiNi shape memory alloy*, Archives of Mechanics, **51**, 6, 649–663, 1999.
22. S.P. GADAJ, W.K. NOWACKI, E.A. PIECZYSKA, *Temperature evolution in deformed shape memory alloy*, Infrared Physics & Technology, **43**, 151–155, 2002.
23. C. GRABE, O.T. BRUHNS, *On the viscous and strain rate dependent behavior of polycrystalline NiTi*, International Journal of Solids and Structures, **45**, 1876–1895, 2008.
24. W. CHEN, B. SONG, *Temperature dependence of a NiTi shape memory alloy's superelastic behavior at a high strain rate*, Journal of Mechanics of Materials and Structures, **1**, 2, 339–356, 2006.
25. C. LIU, J. JIANG, M. ZOU, *A generalized three-wave method for nonlinear evolution equations*, International Journal of Nonlinear Sciences & Numerical Simulation, **11**, 489–494, 2010.
26. F. ČMIEL, J. SOLAŘ, *Termographical measurement of the surface temperature and emissivity of glossy materials using the method of four points*, Advanced Materials Research, **1122**, 195–200, 2015.
27. R. KAPOOR, S. NEMAT-NASSER, *Determination of temperature rise during high strain rate deformation*, Mechanics of Materials, **27**, 1–12, 1998.
28. C. LEXCELLENT, M.R. LAYDI, V. TAILLEBOT, *Analytical prediction of the phase transformation onset zone at a crack tip of a shape memory alloy exhibiting asymmetry between tension and compression*, International Journal of Fracture, **169**, 1, 1–13, 2010.
29. L. WANG, *Foundations of Stress Waves*, 1st ed., Elsevier, Oxford, 2007.

Received August 9, 2017; revised version April 28, 2018.

---